

# Slow modes in Keplerian disks

Scott Tremaine

*Princeton University Observatory, Peyton Hall,  
Princeton, NJ 08544-1001*

tremaine@astro.princeton.edu

## ABSTRACT

Low-mass disks orbiting a massive body can support “slow” normal modes, in which the eigenfrequency is much less than the orbital frequency. Slow modes are lopsided, i.e., the azimuthal wavenumber  $m = 1$ . We investigate the properties of slow modes, using softened self-gravity as a simple model for collective effects in the disk. We employ both the WKB approximation and numerical solutions of the linear eigenvalue equation. We find that all slow modes are stable. Discrete slow modes can be divided into two types, which we label g-modes and p-modes. The g-modes involve long leading and long trailing waves, have properties determined by the self-gravity of the disk, and are only present in narrow rings or in disks where the precession rate is dominated by an external potential. In contrast, the properties of p-modes are determined by the interplay of self-gravity and other collective effects. P-modes involve both long and short waves, and in the WKB approximation appear in degenerate leading/trailing pairs. Disks support a finite number—sometimes zero—of discrete slow modes, and a continuum of singular modes.

*Subject headings:* celestial mechanics, stellar dynamics — stars: formation — galaxies: nuclei

## 1. Introduction

Disks orbiting massive bodies are found in many astrophysical systems. These may be composed of gas (surrounding protostars, compact objects in binary star systems, or black holes in galactic nuclei), dust (a component of protoplanetary disks), solid bodies (planetary rings and planetesimal disks), or stars (galactic nuclei). Normally the disk mass  $M_d$  in these systems is much less than the central mass  $M$ , so that the gravitational potential is nearly Keplerian. A special feature of the Keplerian potential is that eccentric orbits do not precess. This feature arises from a 1:1 resonance between the radial and azimuthal frequencies, and implies that the evolution of the eccentricity distribution in an isolated Keplerian disk is determined by the collective effects in the disk (self-gravity, pressure, collisions, viscosity, etc.), no matter how small these may be. Thus we expect

that Keplerian disks may be capable of supporting a set of normal modes with eigenfrequency  $\omega$  much less than the Keplerian orbital frequency  $\Omega(r) = (GM/r^3)^{1/2}$ , and properties determined by weak collective effects in the disk. In the linear limit these modes have azimuthal wavenumber  $m = 1$ . We shall call them “slow” modes.

The goal of this paper is to investigate slow modes in Keplerian disks. In this Section we provide an introduction and orientation based on the WKB approximation. We shall find that in many cases slow modes have scales comparable to the size of the disk, so that the WKB analysis must be supplemented by numerical calculations of large-scale modes. We soften the self-gravity of the disk to mimic the effects of pressure in fluid disks and velocity dispersion in collisionless disks, and derive the integral eigenvalue equation that describes large-scale slow modes in §II. We discuss the numerical solution of this integral equation for several disk models in §III. Section IV contains a discussion of earlier related work, and §V contains conclusions.

### 1.1. The precession rate

We employ cylindrical coordinates  $(r, \phi, z)$  with origin at the central mass  $M$ , and approximate the unperturbed disk as razor-thin, with surface density  $\Sigma_d(r)$  in the  $z = 0$  plane. We assume that the disk mass is small,  $M_d/M \sim \Sigma_d r^2/M \sim \epsilon \ll 1$ . The unperturbed disk material orbits in the axisymmetric potential

$$\Phi(r) = -\frac{GM}{r} + \Phi_d(r) + \Phi_e(r), \quad (1)$$

where  $\Phi_d(r)$  is the potential arising from the self-gravity of the disk and  $\Phi_e(r)$  is the non-Keplerian potential from any external source, and both are assumed to be  $O(\epsilon)$ .

For nearly circular orbits, the azimuthal and radial frequencies  $\Omega > 0$  and  $\kappa > 0$  are given by (e.g. Binney and Tremaine 1987)

$$\begin{aligned} \Omega^2(r) &= \frac{GM}{r^3} + \frac{1}{r} \frac{d}{dr} (\Phi_d + \Phi_e), \\ \kappa^2(r) &= \frac{GM}{r^3} + \frac{d^2}{dr^2} (\Phi_d + \Phi_e) + \frac{3}{r} \frac{d}{dr} (\Phi_d + \Phi_e). \end{aligned} \quad (2)$$

The line of apsides of an eccentric test-particle orbit subjected only to gravity precesses at a rate

$$\begin{aligned} \dot{\varpi} &= \Omega - \kappa \\ &= -\frac{1}{2\Omega(r)} \left( \frac{2}{r} \frac{d}{dr} + \frac{d^2}{dr^2} \right) (\Phi_d + \Phi_e) + O(\epsilon^2), \end{aligned} \quad (3)$$

where from now on  $\Omega(r)$  is assigned the Keplerian value,  $(GM/r^3)^{1/2}$ .

### 1.2. The Kuzmin disk

Several of our examples will be based on the Kuzmin disk, which has surface density and potential (e.g. Binney and Tremaine 1987)

$$\Sigma_d(r) = \frac{aM_d}{2\pi(r^2 + a^2)^{3/2}}, \quad \Phi_d(r) = -\frac{GM_d}{(r^2 + a^2)^{1/2}}, \quad (4)$$

where  $M_d$  is the disk mass and  $a$  is the disk scale length. Using equation (3), the precession rate due to the Kuzmin disk is

$$\dot{\omega}_d = -\frac{3GM_d a^2}{2\Omega(r)(r^2 + a^2)^{5/2}}, \quad (5)$$

for  $M_d \ll M$ . The precession rate is negative at all radii, approaches zero as  $r^{3/2}$  for small radii and as  $r^{-7/2}$  at large radii, and has a single extremum at  $r_0 = (\frac{3}{7})^{1/2}a = 0.6547a$  where  $\dot{\omega}(r_0) = -0.3257(M_d/M)(GM/a^3)^{1/2}$ .

### 1.3. The WKB approximation

We can write the linearized surface-density response of the disk as a superposition of terms of the form  $\Sigma(r, \phi, t) = A(r) \exp \{i[\int^r k(r)dr + m\phi - \omega t]\}$ , where  $m$  is the azimuthal wavenumber,  $k(r)$  is the radial wavenumber, and  $\omega$  is the frequency. In the WKB or tight-winding approximation where  $|kr| \gg 1$ , the dispersion relation between  $k(r)$  and  $\omega$  depends only on the local properties of the disk, and can be derived analytically for both fluid and collisionless disks.

For a barotropic fluid disk with sound speed  $c(r)$ , the WKB dispersion relation reads (Safronov 1960; Binney and Tremaine 1987)

$$(\omega - m\Omega)^2 = \kappa^2 - 2\pi G\Sigma_d|k| + k^2 c^2. \quad (6)$$

This relation implies that the disk is locally stable to axisymmetric ( $m = 0$ ) disturbances if and only if

$$Q \equiv \frac{c\kappa}{\pi G\Sigma_d} > 1. \quad (7)$$

For thin, low-mass disks we have  $c \ll \Omega r$  and  $\Sigma_d \ll M/r^2$ , so that in general the dispersion relation (6) can only be satisfied if  $|kr| \gg 1$ , which justifies the use of the WKB approximation. However, the special case of  $m = 1$  disturbances in a nearly Keplerian disk is different. Using equation (3) the dispersion relation can be rewritten in the form

$$\omega = \dot{\omega} + \frac{\pi G\Sigma_d|k|}{\Omega} - \frac{k^2 c^2}{2\Omega} + \frac{1}{\Omega} O(\dot{\omega}^2, \omega^2). \quad (8)$$

Since we are interested in slow modes in nearly Keplerian disks, the terms of order  $\dot{\omega}^2$ ,  $\omega^2$  can be dropped. At a given radius, the maximum value of  $\omega$  is attained at wavenumber  $|k| \equiv k_0 = \pi G\Sigma_d/c^2$ .

Let us neglect the effects of pressure for the moment, by dropping the term proportional to  $c^2$  in equation (8). Thus the WKB dispersion relation for slow waves dominated by self-gravity becomes

$$\omega = \dot{\omega} + \frac{\pi G \Sigma_d |k|}{\Omega}. \quad (9)$$

Since  $\dot{\omega}/\Omega = O(\Sigma_d r^2/M)$  for isolated disks, in general the two terms on the right side of (8) are only comparable if  $|kr| \sim 1$ ; thus slow gravity-dominated waves must be large-scale (i.e. the WKB approximation is *not* satisfied) and have eigenfrequency  $\omega = O(\dot{\omega})$ . The neglect of the pressure term is valid for such waves so long as  $G \Sigma_d r \gg c^2$ , or  $\mathcal{M} \gg Q$ , where  $\mathcal{M}(r) \equiv \Omega r/c$  is the Mach number.

Next consider a collisionless disk with a Schwarzschild distribution function having radial velocity dispersion  $c_R(r)$ . The WKB dispersion relation reads (Kalnajs 1965; Lin and Shu 1966; Binney and Tremaine 1987)

$$(\omega - m\Omega)^2 = \kappa^2 - 2\pi G \Sigma_d |k| \mathcal{F} \left( \frac{\omega - m\Omega}{\kappa}, \frac{k^2 c_R^2}{\kappa^2} \right), \quad (10)$$

where  $\mathcal{F}(s, \chi)$  is the reduction factor. Explicit formulae for the reduction factor are given in the references above. The disk is locally stable to axisymmetric disturbances if and only if (Toomre 1964)

$$Q \equiv \frac{c_R \kappa}{3.36 G \Sigma_d} > 1, \quad (11)$$

which closely resembles equation (7). For  $m = 1$  disturbances in a nearly Keplerian disk, the dispersion relation (10) simplifies to

$$\omega = \dot{\omega} + \frac{\pi G \Sigma_d |k|}{\Omega} \mathcal{F}_K \left( \frac{k^2 c_R^2}{\Omega^2} \right), \quad (12)$$

in which

$$\mathcal{F}_K(\chi) = \frac{2}{\chi} e^{-\chi} I_1(\chi), \quad (13)$$

and  $I_1(\chi)$  is a modified Bessel function. At a given radius, the maximum value of  $\omega$  is attained at wavenumber  $|k| \equiv k_0 = 0.7643 \Omega/c_R$ . Since both terms on the right side of (12) scale as the disk surface density  $\Sigma_d$ , for a fixed velocity-dispersion profile the shape of a mode is independent of the disk mass and the eigenfrequency is proportional to the disk mass.

For the moment assume  $\chi \ll 1$ ; then the reduction factor  $\mathcal{F}(\chi) = 1$  and the dispersion relation (12) reduces to (9): we conclude, not surprisingly, that the WKB dispersion relation for slow gravity waves is the same for fluid and collisionless disks. The neglect of the reduction factor is valid for such waves so long as  $\chi \ll 1$  when  $|kr| \sim 1$ , which in turn requires that the Mach number  $\mathcal{M}_R \equiv \Omega r/c_R \gg 1$ .

Many of the properties of waves in collisionless disks can be mimicked by softening the gravitational potential, using  $-Gm/(d^2 + b^2)^{1/2}$  instead of  $-Gm/d$  for the potential due to a mass  $m$

at distance  $d$ . Here the parameter  $b$  is the softening length. This modification yields the WKB dispersion relation (Miller 1971; Erickson 1974; Toomre 1977)

$$\omega = \dot{\varpi}(r) + \frac{\pi G \Sigma_d(r)}{\Omega(r)} |k| \exp(-|k|b). \quad (14)$$

At a given radius, the maximum value of  $\omega$  is attained at wavenumber  $|k| \equiv k_0 = 1/b$ . As in the case of a collisionless disk, both terms on the right side scale as the disk surface density  $\Sigma_d$ , so the eigenfrequency is proportional to the disk mass. In the long-wavelength limit,  $|k|b \ll 1$ , the dispersion relation simplifies once again to equation (9).

By analogy with the theory of WKB waves in galactic disks, we call waves trailing if  $k > 0$  and leading if  $k < 0$ . Long waves have  $|k| < k_0$  and short waves have  $|k| > k_0$ .

We conclude from these approximate arguments that a low-mass, thin disk (by which we mean  $\Sigma_d r^2/M \sim \epsilon \ll 1$ , and  $\mathcal{M} \gg Q$  for a fluid disk, or  $\mathcal{M} \gg 1$  for a collisionless disk) could support slow modes with the following properties: (i) the azimuthal wavenumber  $m = 1$ ; (ii) the dominant collective effect is self-gravity; (iii)  $|kr| = O(1)$ , that is, the wavelength is comparable to the disk radius, the properties of the mode are determined globally rather than locally, and the mode cannot be described accurately with the WKB approximation; (iv) the properties of the mode depend on the disk self-gravity but not on other collective effects; (v) the eigenfrequency is of order  $\epsilon\Omega$ . Many of these conclusions were derived already by Lee and Goodman (1999), in a paper focused mainly on nonlinear waves in nearly Keplerian disks.

Despite conclusion (iii), the WKB approximation provides an invaluable guide to the properties of slow modes. It is useful to plot contours of constant  $\omega$  in the  $(k, r)$  plane. Figure 1 shows such contour plots for the Kuzmin disk discussed in §1.2 and four dispersion relations for slow waves: a disk with softened gravity (eq. 14), a fluid disk (eq. 8), a collisionless disk (eq. 12), and a gravity-dominated disk (eq. 9). Local maxima in the contour plots occur at  $k = \pm k_0$ , and a local minimum at  $k = 0$ .

In these diagrams, a WKB wavepacket travels along a contour of constant  $\omega$ , at a radial speed given by the group velocity  $d\omega/dk$  (Toomre 1969). Long trailing and short leading waves propagate outwards, while long leading and short trailing waves propagate in. In the WKB approximation a mode corresponds to a closed contour in Figure 1 on which the total phase change  $\oint k(r)dr$  over one circuit is an integer multiple of  $2\pi$ , including possible phase shifts at the turning points. The models in the Figure exhibit two types of closed contour:

1. On contours such as C in the upper-left panel, an outward-traveling long trailing wave refracts into an inward-traveling short trailing wave, which in turn refracts back into a long wave. Contours such as B are similar, except that they involve inward-traveling long leading waves and outward-traveling short leading waves. WKB modes of types B and C occur in degenerate pairs. Modes of this kind are not present in the gravity-dominated disk (lower right panel), since this disk supports only long waves. In the Kuzmin disk these modes have  $\omega > 0$ , and

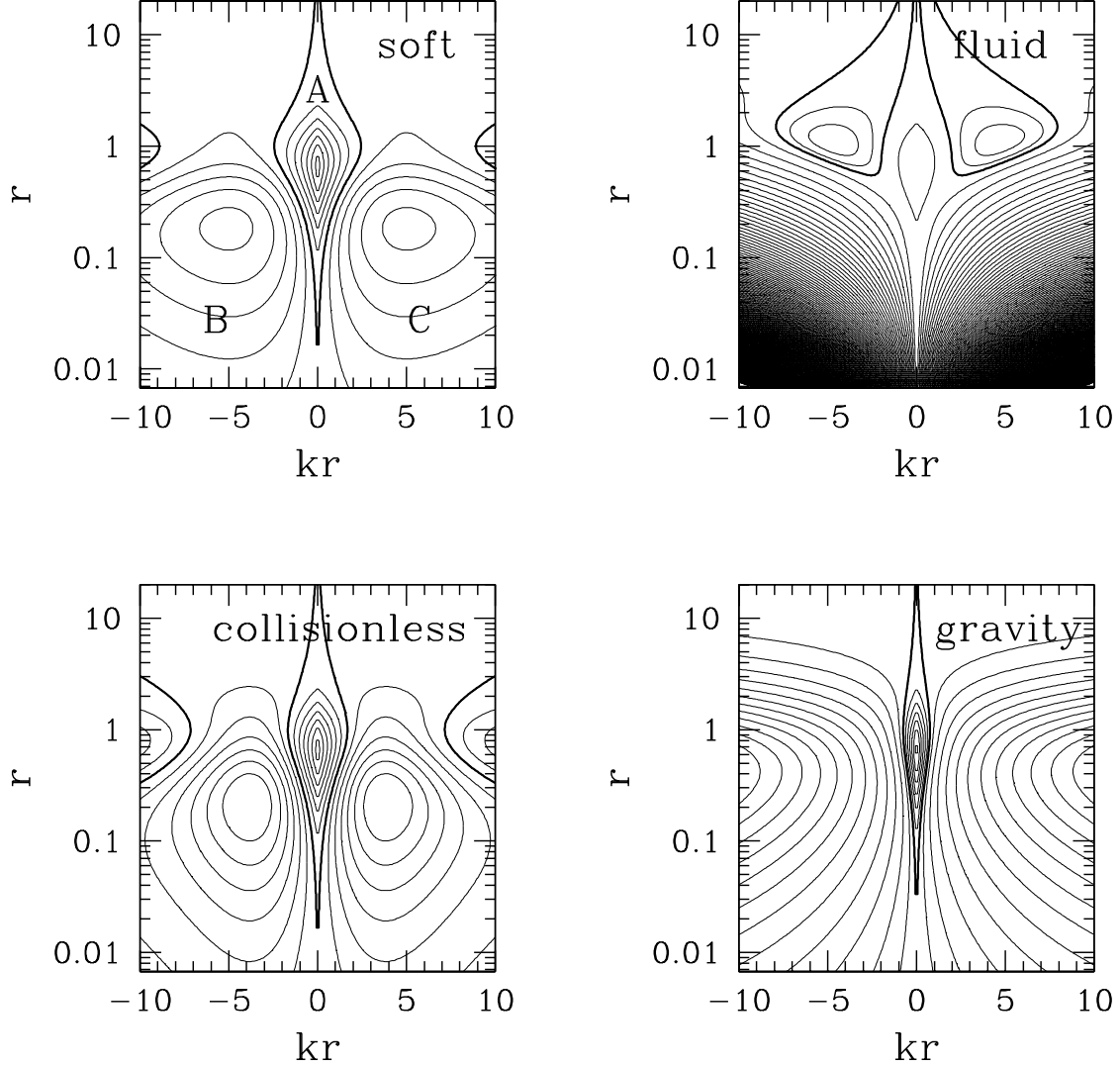


Fig. 1.— Contours of constant frequency  $\omega$  for WKB slow waves in a Kuzmin disk (§1.2), as a function of wavenumber  $kr$  and radius  $r$ . The dispersion relations shown are for a disk with softened gravity (eq. 14), a fluid disk (eq. 8), a collisionless disk (eq. 12), and a gravity-dominated disk (eq. 9). The disk scalelength  $a = 1$ , the softening length  $b = 0.2r$ , the Mach number  $\mathcal{M} = \Omega/cr$  or  $\mathcal{M}_R = \Omega r/c_R$  is the same for the fluid and the collisionless disk and equal to 5 at all radii. Both the gravitational constant  $G$  and the central mass  $M$  are unity; the disk mass  $M_d = 1$  and  $\omega$  scales as  $M_d$  so long as  $b$ ,  $\mathcal{M}_R$  or  $M_d \mathcal{M}^2$  remain invariant. The extrema at  $kr = 0$  are minima. The contours in the right-hand panels are not uniformly spaced.

the modes with the smallest phase change around the contour have the highest frequency and wavenumbers localized near  $\pm k_0$ . We call these *p-modes*, since they require the presence of pressure, velocity dispersion, or softening.

2. In contrast, closed contours such as A involve only long waves, and involve reflection of an outward-traveling long trailing wave into an inward-traveling long leading wave, which then reflects back to long trailing. These modes are present in all four panels; their properties are similar in all panels since they depend only on the surface-density distribution in the disk and not other collective effects. In the Kuzmin disk these modes have  $\omega < 0$ , and the modes with the fewest nodes have the most negative values of  $\omega$ . The WKB approximation is highly suspect for waves of this kind since  $|kr| \lesssim 1$ , so numerical mode calculations are required. We call these *g-modes*, since self-gravity is the only collective effect involved.

Figure 1 suggests that the WKB dispersion relation for collisionless Keplerian disks can be reproduced quite well by disks with softened gravity (Erickson 1974; Toomre 1977); and at least the qualitative features of the dispersion relation in fluid disks are similar as well. Therefore, in our numerical mode calculations we shall soften the self-gravity of the disk but neglect other collective effects.

## 2. Linear perturbation theory

In this Section we derive the linear eigenvalue equation for slow modes in disks with softened gravity. We write the surface density, velocity and potential of the perturbed disk as  $\Sigma_d(r) + \Sigma_a(\mathbf{r}, t)$ ,  $\mathbf{v}_d(\mathbf{r}) + \mathbf{v}_a(\mathbf{r}, t) = r\Omega\hat{\phi} + u_a(\mathbf{r}, t)\hat{\mathbf{r}} + v_a(\mathbf{r}, t)\hat{\phi}$ ,  $\Phi_d(r) + \Phi_a(\mathbf{r}, t)$ . The linearized Euler and continuity equations read

$$\begin{aligned} \frac{\partial \mathbf{v}_a}{\partial t} + (\mathbf{v}_d \cdot \nabla) \mathbf{v}_a + (\mathbf{v}_a \cdot \nabla) \mathbf{v}_d &= -\nabla \Phi_a, \\ \frac{\partial \Sigma_a}{\partial t} + \nabla \cdot (\Sigma_d \mathbf{v}_a + \Sigma_a \mathbf{v}_d) &= 0. \end{aligned} \quad (15)$$

We write the perturbation variables  $(u_a, v_a, \Sigma_a, \Phi_a)$  in the form  $X_a(r, \phi, t) = X_a^m(r) \exp[i(m\phi - \omega t)]$ . Equations (15) become

$$\begin{aligned} i(m\Omega - \omega)u_a^m - 2\Omega v_a^m &= -\frac{d\Phi_a^m}{dr}, \\ \frac{\kappa^2}{2\Omega}u_a^m + i(m\Omega - \omega)v_a^m &= -\frac{im}{r}\Phi_a^m, \\ i(m\Omega - \omega)\Sigma_a^m &= -\frac{1}{r}\frac{d}{dr}(r\Sigma_d u_a^m) - \frac{im}{r}\Sigma_d v_a^m. \end{aligned} \quad (16)$$

The first two of these can be solved to yield

$$u_a^m = -\frac{i}{D} \left[ (m\Omega - \omega) \frac{d}{dr} + \frac{2m\Omega}{r} \right] \Phi_a^m,$$

$$v_a^m = \frac{1}{D} \left[ \frac{\kappa^2}{2\Omega} \frac{d}{dr} + \frac{m}{r} (m\Omega - \omega) \right] \Phi_a^m, \quad (17)$$

where

$$D = \kappa^2 - (m\Omega - \omega)^2. \quad (18)$$

### 2.1. Nearly Keplerian disks

We now specialize to slow perturbations in nearly Keplerian disks. Thus we assume that the disk potential and any external non-Keplerian potential satisfy  $|\Phi_d, \Phi_e|/(GM/r) = O(\epsilon) \ll 1$ , and that the azimuthal wavenumber  $m = 1$ . Furthermore we assume  $|\omega|/\Omega = O(\epsilon)$ , for the reasons given in §1.3. Using equation (3), the denominator  $D$  (eq. 18) becomes

$$D = 2\Omega(\omega - \dot{\varpi}) + O(\epsilon^2); \quad (19)$$

and equations (17) become

$$\begin{aligned} u_a^1 &= -\frac{i}{2(\omega - \dot{\varpi})} \left( \frac{d\Phi_a^1}{dr} + \frac{2\Phi_a^1}{r} \right) \\ v_a^1 &= \frac{1}{4(\omega - \dot{\varpi})} \left( \frac{d\Phi_a^1}{dr} + \frac{2\Phi_a^1}{r} \right), \end{aligned} \quad (20)$$

with fractional error  $O(\epsilon)$ . Thus to leading order in  $\epsilon$ ,

$$u_a^1 = -2iv_a^1, \quad (21)$$

which is simply the relation between the radial and azimuthal non-circular velocities for a nearly circular Keplerian orbit. The Keplerian eccentricity  $e_K$  is related to the perturbed velocities by

$$u_a^1 = -2iv_a^1 = -i \left( \frac{GM}{r} \right)^{1/2} e_K \exp(-i\varpi). \quad (22)$$

We may use equation (21) to eliminate the radial velocity from the continuity equation (the last of eqs. 16); to leading order in  $\epsilon$  this now reads

$$\Omega \Sigma_a^1 = \frac{2}{r} \frac{d}{dr} (r \Sigma_d v_a^1) - \frac{\Sigma_d v_a^1}{r} = 2 \frac{d}{dr} (\Sigma_d v_a^1) + \frac{\Sigma_d v_a^1}{r}. \quad (23)$$

The second of equations (20) can be rewritten as

$$(\omega - \dot{\varpi}) v_a^1 = \frac{1}{4} \frac{d\Phi_a^1}{dr} + \frac{\Phi_a^1}{2r}. \quad (24)$$

Equations (23) and (24), together with Poisson's equation relating  $\Phi_a^1$  and  $\Sigma_a^1$ , describe the slow modes of Keplerian disks when self-gravity is the only collective effect.



## 2.2. Potential theory

Poisson's equation can be written as

$$\Phi_a^m(r) = \int_0^\infty dr' r' P_m(r, r') \Sigma_a^m(r'); \quad (25)$$

the same relation, with  $m = 0$ , also holds between the potential  $\Phi_d$  and the surface density  $\Sigma_d$  of the unperturbed disk. The kernel in equation (25) is

$$P_m(r, r') = -\frac{\pi G}{r_>} b_{1/2}^{(m)}(r_</r_>) + \frac{\pi G r}{r'^2} (\delta_{m1} + \delta_{m,-1}). \quad (26)$$

Here  $r_< = \min(r, r')$ ,  $r_> = \max(r, r')$ , and the second term is the indirect potential arising from the motion of the central body in response to the disk perturbation. The Laplace coefficient

$$b_{1/2}^{(m)}(\alpha) = \frac{2}{\pi} \int_0^\pi \frac{\cos m\theta d\theta}{(1 - 2\alpha \cos \theta + \alpha^2)^{1/2}} \quad (27)$$

(Murray and Dermott 1999). In particular,

$$b_{1/2}^{(0)}(\alpha) = \frac{4}{\pi} K(\alpha), \quad b_{1/2}^{(1)}(\alpha) = \frac{4}{\pi \alpha} [K(\alpha) - E(\alpha)], \quad (28)$$

where  $K(\alpha)$  and  $E(\alpha)$  are complete elliptic integrals. We shall use the relations

$$\frac{dE(\alpha)}{d\alpha} = \frac{E(\alpha) - K(\alpha)}{\alpha}, \quad \frac{dK(\alpha)}{d\alpha} = \frac{E(\alpha)}{\alpha(1 - \alpha^2)} - \frac{K(\alpha)}{\alpha}. \quad (29)$$

The Laplace coefficients are singular at  $\alpha = 1$ ,

$$b_{1/2}^{(0)}(1 - \delta) = -\frac{2}{\pi} \ln \delta + \frac{2}{\pi} \ln 8 + O(\delta \ln \delta); \quad b_{1/2}^{(1)}(1 - \delta) = -\frac{2}{\pi} \ln \delta + \frac{2}{\pi} (\ln 8 - 2) + O(\delta \ln \delta). \quad (30)$$

We can soften the logarithmic singularity by replacing  $\ln \delta$  by  $\frac{1}{2} \ln(\delta^2 + \beta^2)$  where  $\beta$  is the softening parameter; the actual softening length is then radius-dependent,  $b = \beta r$ . If we adopt this prescription then we must soften the stronger singularities that arise from derivatives of  $\ln \delta$  by differentiating  $\frac{1}{2} \ln(\delta^2 + \beta^2)$ . Thus

$$\ln \delta \rightarrow \frac{1}{2} \ln(\delta^2 + \beta^2), \quad \frac{1}{\delta} \rightarrow \frac{\delta}{\delta^2 + \beta^2}, \quad \frac{1}{\delta^2} \rightarrow \frac{\delta^2 - \beta^2}{(\delta^2 + \beta^2)^2}. \quad (31)$$

A full description of the softening procedure follows equations (45) and (53).

## 2.3. The eigenvalue equation

Combining equations (23), (24) and (25), we get

$$[\omega - \dot{\omega}(r)] v_a^1(r) = \int \frac{r' dr'}{\Omega(r')} \left[ \frac{1}{4} \frac{\partial}{\partial r} P_1(r, r') + \frac{1}{2r} P_1(r, r') \right] \left[ 2 \frac{d}{dr'} \Sigma_d(r') v_a^1(r') + \frac{\Sigma_d(r') v_a^1(r')}{r'} \right]. \quad (32)$$

This can be recast by writing

$$y(r) = \left[ \frac{r^2 \Sigma_d(r)}{\Omega(r)} \right]^{1/2} v_a^1(r); \quad (33)$$

we then integrate by parts, using the fact that  $\Omega(r) \propto r^{-3/2}$ , to obtain

$$\omega y(r) = \dot{\varpi}(r) y(r) + \int \frac{dr'}{r'} K(r, r') y(r'), \quad (34)$$

where the kernel

$$K(r, r') = -2 \left[ \frac{\Sigma_d(r) \Sigma_d(r')}{\Omega(r) \Omega(r')} \right]^{1/2} \left( 1 + \frac{1}{2} \frac{\partial}{\partial \ln r} \right) \left( 1 + \frac{1}{2} \frac{\partial}{\partial \ln r'} \right) P_1(r, r'). \quad (35)$$

The contribution of the indirect potential in equation (26) to  $K(r, r')$  vanishes, and the remaining component of  $P_1(r, r')$  is symmetric in  $r$  and  $r'$ , so  $K(r, r')$  is also symmetric.

Since the kernel is real and symmetric, the right side of equation (34) can be regarded as a linear, Hermitian operator acting on  $y(r')$ . From the properties of Hermitian operators we can conclude (e.g., Courant and Hilbert 1953) that (i) the eigenvalues  $\omega$  are real; thus *all slow disturbances are stable*; (ii) the eigenfunctions  $y_n(r)$  associated with different eigenvalues  $\omega_n$  are orthogonal with respect to the inner product  $(y, z) \equiv \int y^*(r) z(r) dr/r$ , that is,  $(y_n, y_m) = 0$  if  $\omega_n \neq \omega_m$ .

Since the kernel is real, the solutions  $y(r)$  or  $v_a^1(r)$  can be assumed to be real. In this case it proves useful to redefine the eccentricity  $e_K$  (eq. 22) by the relation

$$v_a^1 = \frac{1}{2} \left( \frac{GM}{r} \right)^{1/2} e_K(r); \quad (36)$$

so that  $e_K(r)$  is real but can have either sign.

Using equations (26), (28) and (29) we can derive alternative forms for the kernel,

$$\begin{aligned} K(r, r') &= -\frac{\pi G}{2} \left[ \frac{\Sigma_d(r) \Sigma_d(r')}{r r' \Omega(r) \Omega(r')} \right]^{1/2} \alpha^{1/2} \left( \alpha^2 \frac{d^2}{d\alpha^2} + 2\alpha \frac{d}{d\alpha} - 2 \right) b_{1/2}^{(1)}(\alpha), \\ &= -G \left[ \frac{\Sigma_d(r) \Sigma_d(r')}{r r' \Omega(r) \Omega(r')} \right]^{1/2} C(\alpha), \end{aligned} \quad (37)$$

where  $\alpha = r_{<}/r_{>}$  and

$$C(\alpha) = 2\alpha^{-1/2} \left[ \frac{2(1 - \alpha^2 + \alpha^4)}{(1 - \alpha^2)^2} E(\alpha) - \frac{2 - \alpha^2}{1 - \alpha^2} K(\alpha) \right]. \quad (38)$$

The precession rate is given by equations (3) and (25) and can be written as

$$\dot{\varpi} = \dot{\varpi}_d + \dot{\varpi}_e = \int \frac{dr'}{r'} Q(r, r') + \dot{\varpi}_e. \quad (39)$$

Here  $\dot{\omega}_d$  and  $\dot{\omega}_e$  are the precession rates from the self-gravity of the disk and from external sources (due to the potentials  $\Phi_d$  and  $\Phi_e$  respectively). The kernel is

$$\begin{aligned} Q(r, r') &= \frac{\pi G r'^{3/2} \Sigma_d(r')}{2\Omega(r) r^{5/2}} \alpha^{3/2} \left( \alpha \frac{d^2}{d\alpha^2} + 2 \frac{d}{d\alpha} \right) b_{1/2}^{(0)}(\alpha) \\ &= \frac{G \Sigma_d(r') r'^{3/2}}{\Omega(r) r^{5/2}} D(\alpha), \end{aligned} \quad (40)$$

where

$$D(\alpha) = 2\alpha^{1/2} \left[ \frac{1 + \alpha^2}{(1 - \alpha^2)^2} E(\alpha) - \frac{1}{1 - \alpha^2} K(\alpha) \right]. \quad (41)$$

For the sake of simplicity we shall simply assume that any external precession mimics the precession rate due to the disk itself, that is,  $\dot{\omega}_e(r) = f \dot{\omega}_d(r)$  where  $f$  is a constant. In this case the external precession can be eliminated if we replace the eigenfrequency  $\omega$  by  $\omega(1 + f)$  and replace the integral eigenvalue equation (34) by

$$\omega y(r) = \dot{\omega}_d(r) y(r) + \lambda \int \frac{dr'}{r'} K(r, r') y(r'), \quad (42)$$

where  $\lambda = (1 + f)^{-1}$ .

The behavior of  $C(\alpha)$  and  $D(\alpha)$  as  $\alpha \rightarrow 0$  is given by

$$C(\alpha) \rightarrow \frac{15\pi}{8} \alpha^{7/2}, \quad D(\alpha) \rightarrow \frac{3\pi}{2} \alpha^{5/2}. \quad (43)$$

Both functions are singular at  $\alpha = 1$ : if we write  $x \equiv -\log \alpha > 0$  then

$$\begin{aligned} C(\alpha) &= \frac{1}{x^2} + \frac{15}{8} \log \frac{x}{8} + \frac{179}{48} + O(x), \\ D(\alpha) &= \frac{1}{x^2} + \frac{3}{8} \log \frac{x}{8} + \frac{11}{48} + O(x). \end{aligned} \quad (44)$$

Figure 2 shows the behavior of  $C(\alpha)$  and  $D(\alpha)$ ; for clarity we have removed the dominant singularity by plotting  $c(\alpha) \equiv x^2 C(\alpha)$  and  $d(\alpha) \equiv x^2 D(\alpha)$ .

The eigenvalue equation simplifies considerably in the case of narrow rings: we can replace  $C(\alpha)$  and  $D(\alpha)$  by the leading term in equations (44) and need not distinguish  $r$  from  $r'$  except where they occur in rapidly varying functions such as  $\Sigma_d(r)$  and  $\dot{\omega}(r)$ . Equations (33) and (39) become

$$\begin{aligned} [\omega - \dot{\omega}(r)] v_a^1(r) &= -\frac{G}{\Omega} \int \frac{dr'}{(r - r')^2} \Sigma_d(r') v_a^1(r'), \\ \dot{\omega}(r) &= \frac{G}{\Omega} \int \frac{dr'}{(r - r')^2} \Sigma_d(r'), \end{aligned} \quad (45)$$

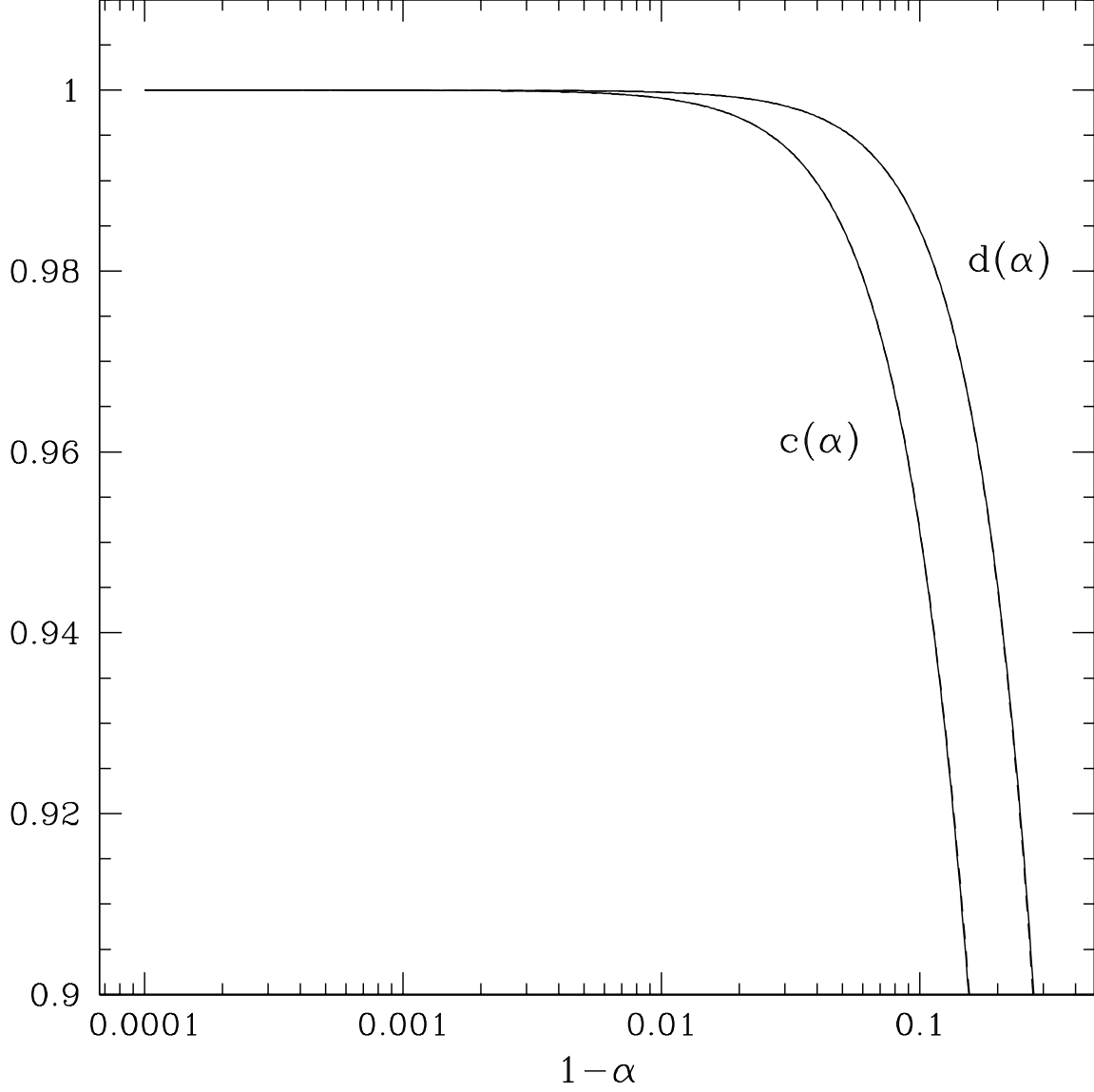


Fig. 2.— The functions  $C(\alpha)$  and  $D(\alpha)$  (eqs. 38 and 41). The dominant singularity has been removed by plotting  $c(\alpha) \equiv x^2 C(\alpha)$  and  $d(\alpha) \equiv x^2 D(\alpha)$ , where  $x = -\log \alpha$  (note that  $\alpha < 1$  so  $x > 0$ ). The plot also contains dashed lines that almost coincide with the solid lines. These are the approximations used in the numerical integration scheme; the quantities plotted are  $x^2 w_K(x)$  (eq. 48) and  $x^2 w_Q(x)$  (eq. 53).

where  $\Omega$  can be treated as constant. The singular kernel can be softened according to equation (31):

$$\begin{aligned} [\omega - \dot{\omega}(r)]v_a^1(r) &= -\frac{G}{\Omega} \int dr' \Sigma_d(r') v_a^1(r') \frac{(r-r')^2 - b^2}{[(r-r')^2 + b^2]^2}, \\ \dot{\omega}(r) &= \frac{G}{\Omega} \int dr' \Sigma_d(r') \frac{(r-r')^2 - b^2}{[(r-r')^2 + b^2]^2}. \end{aligned} \quad (46)$$

A trivial solution of these equations is  $\omega = 0$ ,  $v_a^1(r) = \text{constant}$ .

## 2.4. Numerical methods

We use similar numerical methods to evaluate the integrals in equations (39) and (42) and discuss both integrals together. We approximate the integrals using an  $N$ -point grid that is uniform in  $u \equiv \log r$ . The main complication is the singularity of the integrands when  $r$  is close to  $r'$ . To handle this singularity, we write the integral in (42) as

$$\int \frac{dr'}{r'} K(r, r') y(r') = \int dv w_K(v - u) \frac{K(e^u, e^v) y(e^v)}{w_K(v - u)} \quad (47)$$

where the weight function is chosen to mimic the singular behavior of the kernel (eq. 44)

$$w_K(x) \equiv \frac{1}{x^2} + \frac{15}{8} \log \frac{|x|}{8} + \frac{179}{48}, \quad (48)$$

Before proceeding further we must soften the kernel to smooth the singularity. We do this by softening the weight function, that is, we replace equation (47) by

$$\int \frac{dr'}{r'} K(r, r') y(r') = \int dv \tilde{w}_K(v - u) \frac{K(e^u, e^v) y(e^v)}{w_K(v - u)}, \quad (49)$$

Following the prescription in equation (31) the softened weight function is

$$\tilde{w}_K(x) \equiv \frac{x^2 - \beta^2}{(x^2 + \beta^2)^2} + \frac{15}{8} \log \frac{(x^2 + \beta^2)^{1/2}}{8} + \frac{179}{48}. \quad (50)$$

It should be stressed that this softened kernel does not correspond to any simple force law between two particles. Its key advantages are that it is numerically convenient when deriving a quadrature rule (see below); it has the correct behavior for softened gravity as  $x \rightarrow 0$ ; and the softened kernel is still symmetric in  $r$  and  $r'$  so the operator remains Hermitian. The softening not only simplifies the numerical evaluation of the integral but also can be used to mimic the effects of velocity dispersion in collisionless disks (cf. Fig. 1).

Now if  $y(r')$  is smooth, the expression  $z(v) \equiv K(e^u, e^v) y(e^v) / w_K(v - u)$  in equation (47) should also be smooth, so to evaluate the contribution to the integral from the interval  $[u_k, u_{k+1}]$  we apply

a four-point quadrature rule of the form

$$\int_{u_k}^{u_{k+1}} dv K(e^u, e^v) y(e^v) = \sum_{j=0}^3 W_j z_{k+j-1}, \quad (51)$$

where  $z_k \equiv z(u_k)$ , and  $z_{-1} = z_{N+1} = 0$ . The weights  $W_j$  are chosen so that the integration is exact if  $z(v)$  is a cubic polynomial, and can be evaluated analytically using the integrals  $\int_a^b v^n \tilde{w}_K(v-u) dv$ ,  $n = 0, \dots, 3$  (Press et al. 1992).

Once the integral in equation (42) has been replaced by a sum, solving the integral equation reduces to finding the eigenvalues and eigenvectors of a symmetric  $N \times N$  matrix, which can be done by standard methods (Press et al. 1992).

A similar strategy is used to evaluate the precession rate: we write the integral in equation (39) as

$$\int \frac{dr'}{r'} Q(r, r') = \int dv w_Q(v-u) \frac{Q(e^u, e^v)}{w_Q(v-u)} \quad (52)$$

where

$$w_Q(x) \equiv \frac{1}{x^2} + \frac{3}{8} \log \frac{|x|}{8} + \frac{11}{48} + \frac{1}{2} x^2; \quad (53)$$

the term  $\frac{1}{2}x^2$  is added to eliminate a zero of  $w_Q(x)$  that would otherwise occur at  $|x| = 1.6712$ , but has no effect near the singularity at  $x = 0$ . We then soften  $w_Q(x)$  to  $\tilde{w}_Q(x)$  and recompute the weights  $W_j$  for the quadrature rule.

### 3. Slow modes of disk models

In our numerical calculations we typically use grids with  $N = 400$ – $800$ . All the significant digits that we quote should be correct in the limit  $N \rightarrow \infty$ .

Numerical mode calculations are more difficult with unsoftened gravity than with softened gravity: the diagonal matrix elements become large when the softening is much less than the grid size, so the accuracy is degraded by roundoff error. Typically the minimum practical softening parameter was  $\beta = 10^{-4}$ .

Our numerical method always yields  $N$  eigenvectors and eigenvalues, but many of these are singular (i.e. the amplitude is much larger at a single grid point than elsewhere). These correspond to the singular (van Kampen) modes that occupy the continuous region of the eigenvalue spectrum.

#### 3.1. The Kuzmin disk

We use units in which  $G = M = a = 1$  (cf. §1.2). We usually employ a grid that covers the range  $-7 \leq \log r \leq 5$ . To account for precession due to the mass inside the innermost grid point, we

divide the disk into “live” and “frozen” components: the frozen component is a Kuzmin disk with  $\log a = -5$  and the same central surface density as the original disk, while the live component is the difference between the original and frozen disks. This approximation is legitimate if the amplitude of the normal mode is negligible for  $\log r \lesssim -5$ . We have checked that our results are not sensitive to the size of the frozen disk.

Since softened self-gravity is the only collective effect, the shape of a mode is independent of the disk mass and the eigenfrequency is proportional to disk mass, so we are free to set  $M_d = 1$  as well, even though the calculations are only valid in real disks if  $M_d \ll M$ .

We classify the modes as g-modes and p-modes, as described in §1.3.

### 3.1.1. *g-modes*

We first examine Kuzmin disks with  $\lambda = 0.1$  and  $\beta \simeq 0$  (actually  $\beta = 10^{-4}$ ), corresponding to the case in which 90% of the precession is due to an external source. The reasons for examining this somewhat artificial case are that (i) these disks do not support p-modes, since gravity is unsoftened; (ii) g-modes are accurately described by the WKB approximation since  $\lambda \ll 1$ . Thus we can both isolate the g-modes and compare their behavior to the analytic discussion in §1.3.

This disk exhibits a rich spectrum of discrete slow modes, which can be sorted by the number of nodes; the modes with  $\leq 8$  nodes are shown in Figure 3 along with their eigenfrequencies. As expected from the WKB analysis, the modes in Figure 3 all have  $\omega < 0$ , and the modes with the fewest nodes have the most negative values of  $\omega$ .

The eigenfrequencies can be predicted using the WKB approximation. The dispersion relation (9) can be modified to include a factor  $\lambda$  that accounts for precession from an external source (cf. eq. 42), and rewritten as

$$|k(r)| = \frac{\Omega(r)}{\pi G \lambda \Sigma_d(r)} [\omega - \dot{\varpi}(r)]. \quad (54)$$

The frequency contour diagram analogous to Figure 1 is shown in the left panel of Figure 4. The g-modes correspond to the contours centered on  $kr = 0$ ,  $r = r_0 = 0.6547$ ; they have turning points at radii  $r_{\pm}$  defined by  $\dot{\varpi}(r_{\pm}) = \omega$ . The eigenfrequencies satisfy the quantum condition that the total phase change around the contour is an integer multiple of  $2\pi$ ,

$$2 \int_{r_-}^{r_+} |k(r)| dr = 2\pi n, \quad n = 1, 2, 3, \dots \quad (55)$$

(there are additional phase shifts of  $\pm \frac{1}{2}\pi$  at the turning points, but these contributions cancel; see, for example, Shu et al. 1990). The right panel of Figure 4 shows the eigenfrequencies of the modes with 0, 1, 2, or 3 nodes, as a function of  $\lambda$ , along with the WKB approximation from equations (54) and (55) for  $n = 1, \dots, 4$ . We see that the WKB approximation predicts the eigenfrequency fairly well for  $\lambda \lesssim 0.3$ . At larger  $\lambda$ , the WKB predictions are seriously in error.

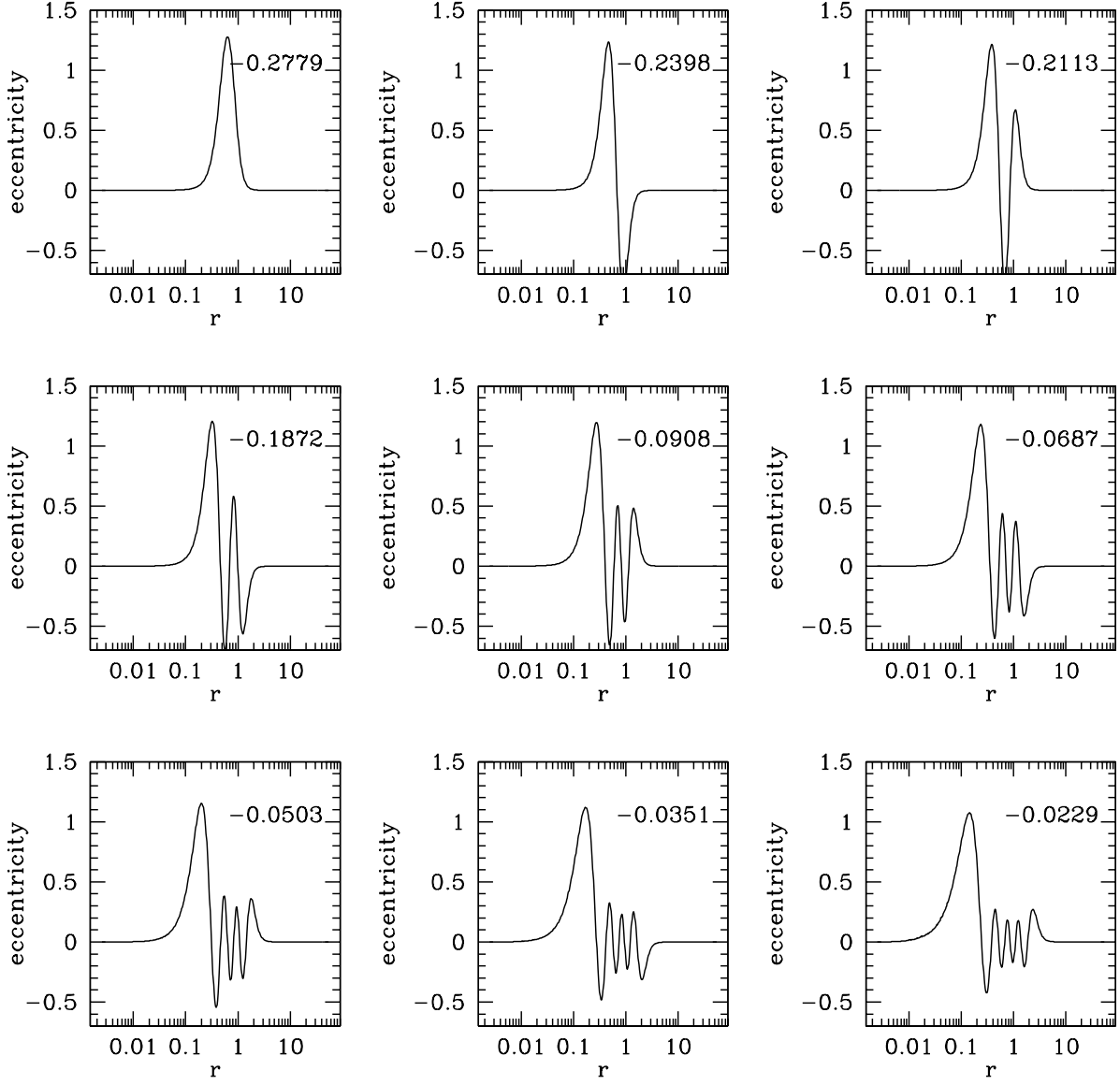


Fig. 3.— Slow g-modes in the Kuzmin disk with  $\lambda = 0.1$  and  $\beta = 0$ . The modes are sorted by the number of nodes. The normalization is chosen so that  $\int e_K^2(r) d \log r = 1$ , where the eccentricity  $e_K(r)$  is defined in equation (36). The number in each panel is the eigenfrequency, in units where  $G = M = M_d = a = 1$ . The eigenfrequency scales as  $(M_d/M)(GM/a^3)^{1/2}$ .



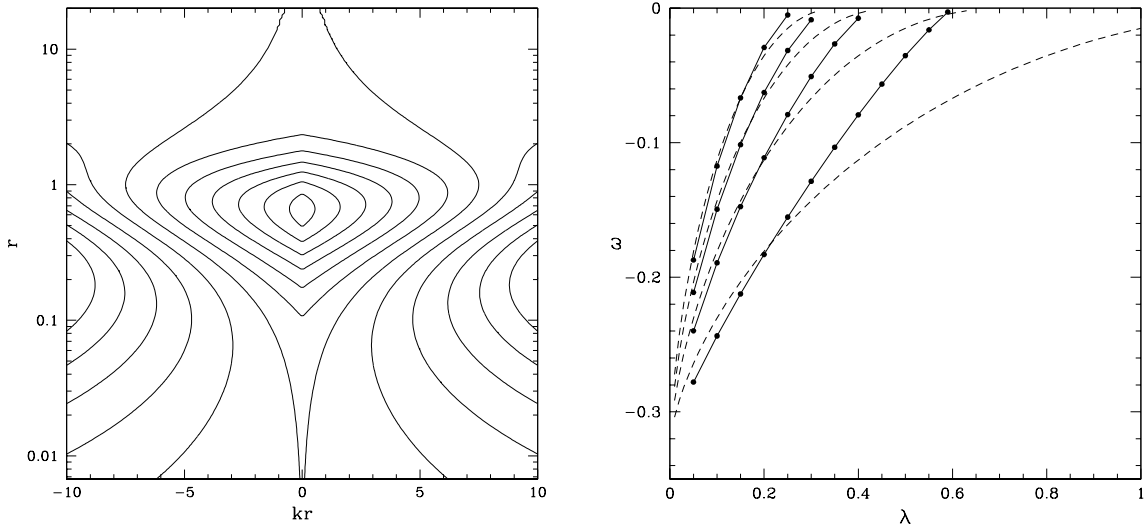


Fig. 4.— (Left) Contours of constant frequency  $\omega$  for WKB slow waves in a Kuzmin disk with  $\lambda = 0.1$  and  $\beta = 0$ , as a function of wavenumber  $kr$  and radius  $r$ . The contours are plotted at intervals of 0.05; the heavy contour is  $\omega = 0$ . The g-modes correspond to the closed contours. (Right) The eigenfrequencies of g-modes with 0, 1, 2, or 3 nodes (bottom to top) for the Kuzmin disk, as a function of  $\lambda$  (solid circles and lines). The dashed lines show the predictions of the WKB approximation (eqs. 54 and 55). There are no slow g-modes for  $\lambda \geq 0.6$ .

As  $\lambda$  increases, the frequency of each g-mode declines in absolute value, until the mode terminates when its frequency reaches zero. There are *no* g-modes in a Kuzmin disk with unsoftened gravity for  $\lambda \geq 0.6$ . In particular, an isolated Kuzmin disk ( $\lambda = 1$ ) does not support g-modes. The reason for this result can be understood qualitatively. As  $\lambda$  increases (i.e. the importance of external precession declines),  $k(r)$  declines as  $\lambda^{-1}$ , (eq. 54) so that the integral on the left side of equation (55) also declines. Eventually this integral is less than  $2\pi$  even for the largest closed contour in Figure 1, at which point the disk cannot support any g-modes.

### 3.1.2. *p-modes*

Next we examine p-modes in isolated Kuzmin disks with softened gravity. Here the WKB analysis is useful even for isolated ( $\lambda = 1$ ) disks so long as  $\beta \ll 1$ , since the characteristic wavenumber is  $k_0 = 1/b = 1/\beta r$ . The WKB analysis predicts that p-modes have  $\omega > 0$ ; that the modes with the fewest nodes have the largest  $\omega$ ; that the modes occur in degenerate pairs; and that the quantum condition is

$$2 \int_{r_-}^{r_+} [k_+(r) - k_-(r)] dr = 2\pi(n - \frac{1}{2}), \quad n = 1, 2, 3, \dots \quad (56)$$

Here  $k_- < k_0 < k_+$  are the two solutions of the dispersion relation (14);  $r_-$  and  $r_+$  are the turning points at which  $k_- = k_+$  for a given  $\omega$ -contour; and the term  $\frac{1}{2}$  on the right side arises because there is a phase shift of  $\frac{1}{2}\pi$  at each turning point (Shu et al. 1990).

Figure 5 shows the predictions of this quantum condition for the Kuzmin disk, as a function of the softening parameter  $\beta = b/r$ . As  $\beta \rightarrow 0$  the eigenfrequencies diverge as  $\beta^{-1}$ , so we have plotted  $\beta\omega$ . The limit point is

$$\lim_{\beta \rightarrow 0} \beta\omega = \frac{5^{5/4}}{2^{5/2} 3^{3/2} e} = 0.093575. \quad (57)$$

We have also plotted the ten largest eigenfrequencies from numerical calculations of the modes. These agree very well with the WKB approximation for small  $\beta$ , and even for  $\beta = 0.3$  the WKB estimates of the eigenfrequencies are accurate within  $\sim 20\%$ . Figure 6 shows the shape of the fundamental ( $n = 1$ ) modes as a function of  $\beta$ . In contrast to the g-modes, the fundamental p-modes can have many nodes, because they are modulated at the high spatial frequency  $k_0$ .

## 3.2. Gaussian rings

In this Section we examine slow modes in rings, by which we mean disks whose surface density approaches zero as  $r \rightarrow \infty$  and as  $r \rightarrow 0$ . As a model for rings we take the surface-density distribution

$$\Sigma_d(r) = \frac{K}{r} \exp \left[ \frac{-(\log r)^2}{2s^2} \right]; \quad (58)$$

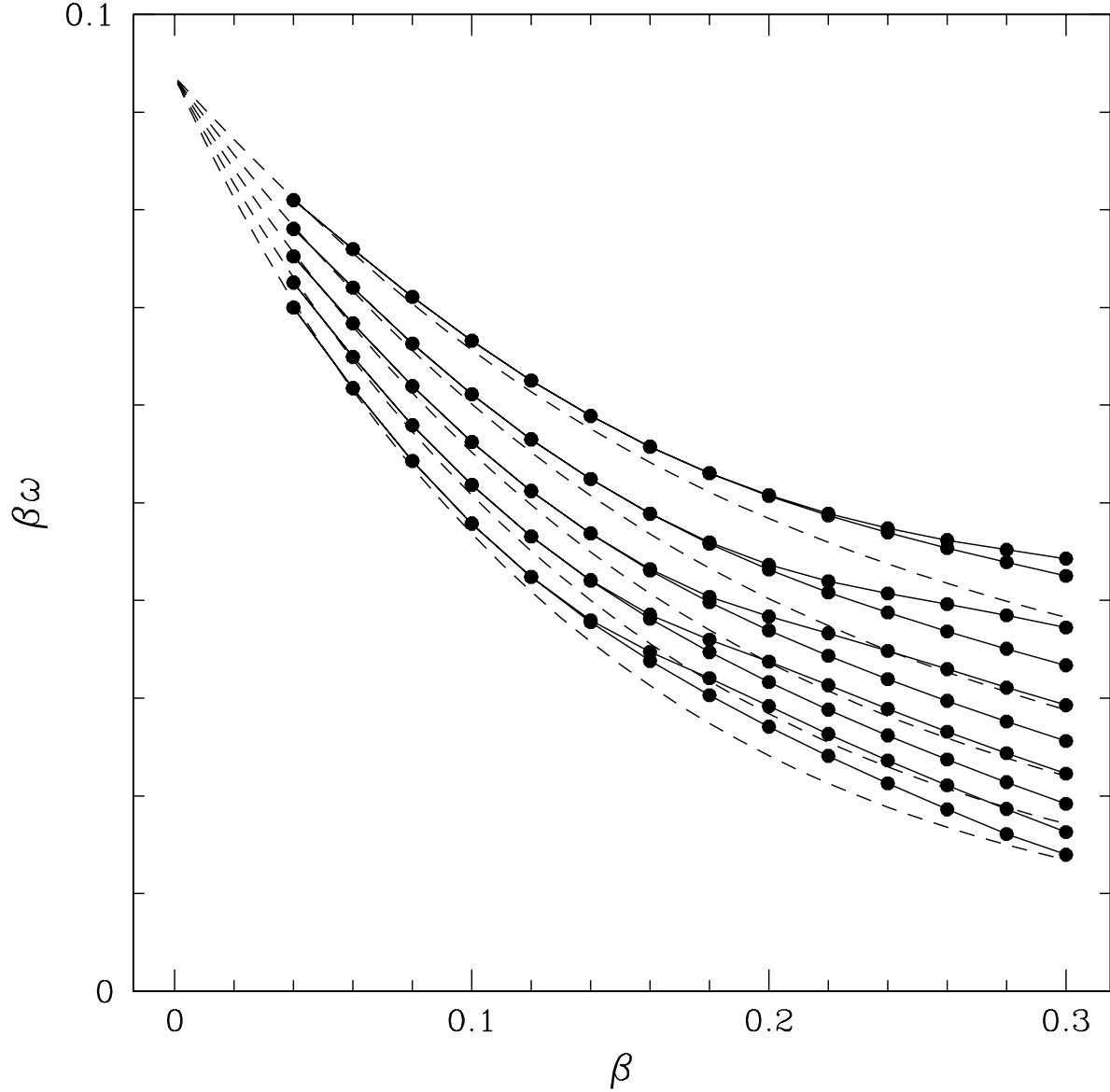


Fig. 5.— Eigenfrequencies of slow p-modes in Kuzmin disks with softened gravity. The units are  $G = M = M_d = a = 1$ . The filled circles and solid curves show numerical solutions for the ten highest eigenfrequencies. The dashed lines show the predictions from the WKB approximation (56) for  $n = 1, \dots, 5$ . In this approximation the modes appear in degenerate leading/trailing pairs. We have plotted  $\beta\omega$  instead of  $\omega$  to expand the vertical scale (cf. eq. 57).

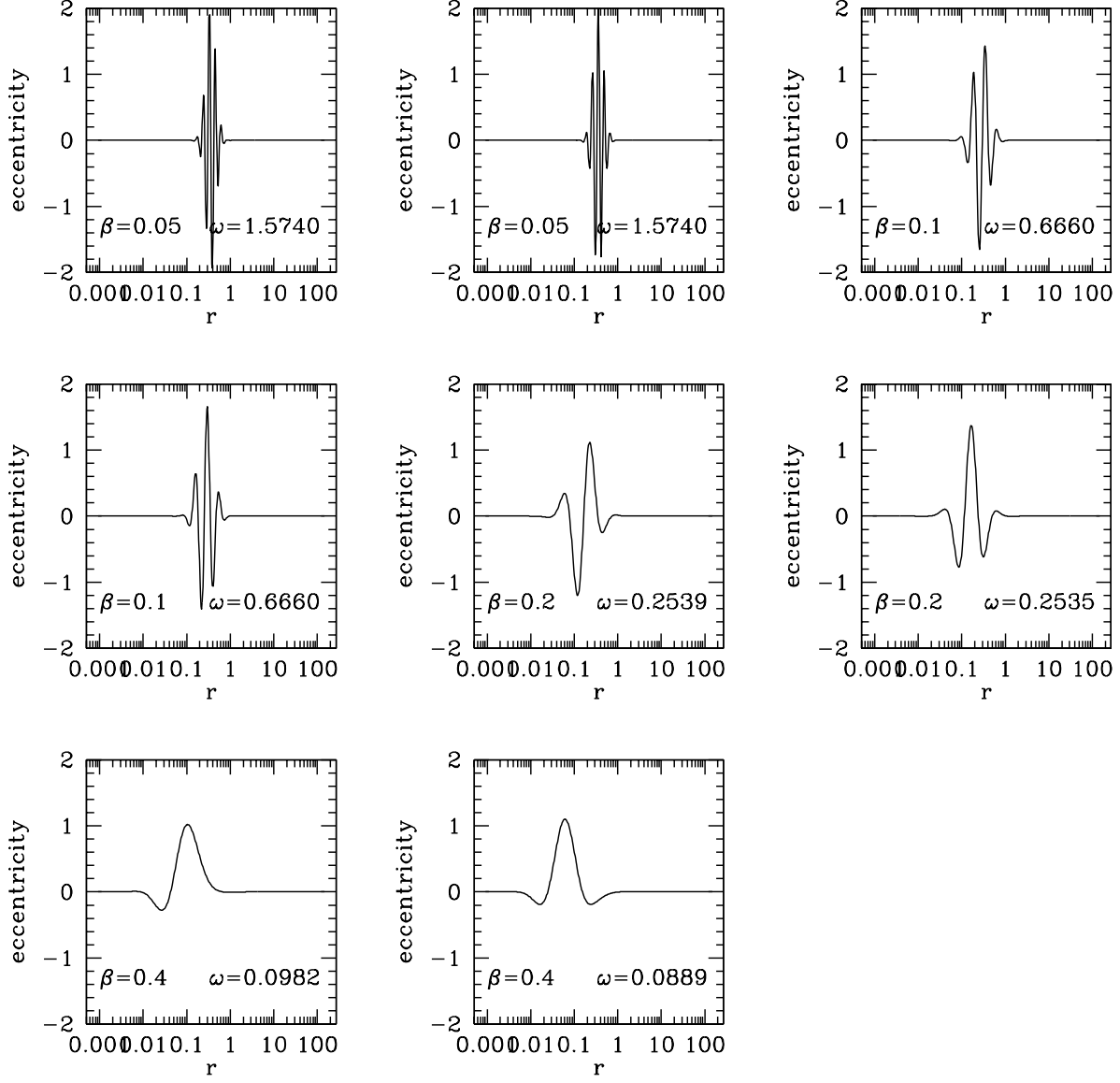


Fig. 6.— Slow p-modes in the isolated Kuzmin disk with softened gravity. The two modes with the highest frequency are shown for disks with  $\beta = 0.05, 0.1, 0.2$ , and  $0.4$ . Note that for  $\beta \ll 1$  the frequencies are nearly degenerate. The normalization is chosen so that  $\int e_K^2(r) d \log r = 1$ , where the eccentricity  $e_K(r)$  is defined in equation (36).

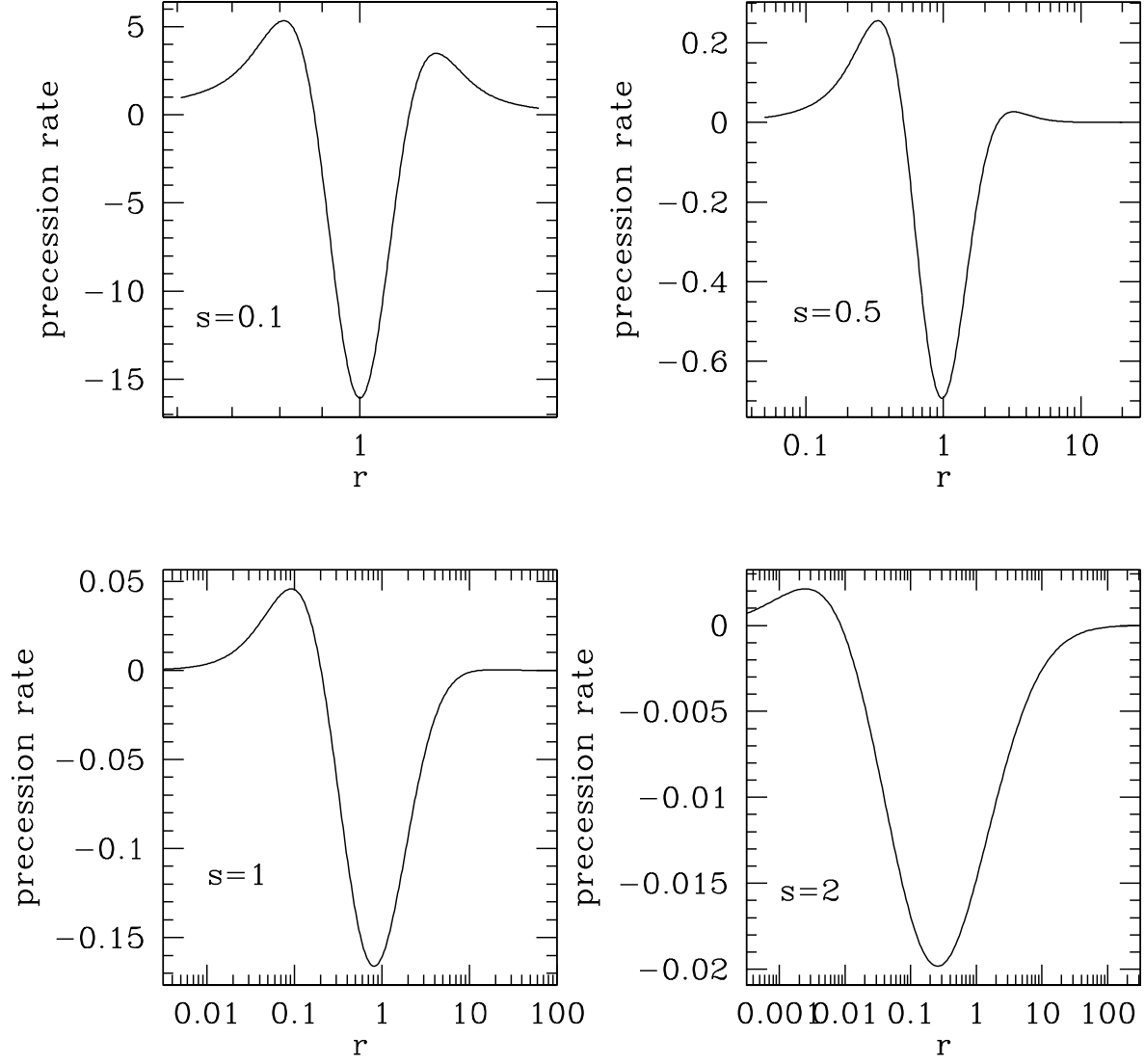


Fig. 7.— The apsidal precession rate  $\dot{\varpi}$  for Gaussian rings with surface-density distribution described by equation (58).

where the constant  $K$  is related to the disk mass by  $M_d = (2\pi)^{3/2} K s \exp(-\frac{1}{2}s^2)$ . The precession rate in these rings is shown in Figure 7. Like the Kuzmin disks, Gaussian rings exhibit a single minimum in the precession rate, but the central minimum is surrounded by shoulders in which the precession rate is positive (prograde).

### 3.2.1. Narrow rings

We showed at the end of §2.3 that there is a trivial slow mode for narrow rings, with zero eigenfrequency and constant velocity perturbation. We can extend this analytic result with numerical solutions of the eigenvalue equation for narrow Gaussian rings.

We find that slow modes for isolated rings with unsoftened gravity are present only if the ring is rather narrow,  $s \lesssim 0.07$ . Only the fundamental mode is non-singular; these are shown in Figure 8. For  $s \lesssim 0.03$  the shape of the fundamental mode is nearly flat, as expected from the trivial solution. At larger  $s$  the amplitude in the outer parts of the ring grows more and more sharply, until for  $s \gtrsim 0.07$  we were unable to find any non-singular modes. The frequency of the fundamental mode declined from  $\omega = 1.1074$  at  $s = 0.01$  to  $\omega = 0.6405$  at  $s = 0.07$ , in units where the ring mass  $M_d = 1$ .

### 3.2.2. Broad rings

We have examined a sequence of broader Gaussian rings, with softening parameter  $\beta = 0.2$  and width  $s = 0.5, 1, 2$ . The three highest-frequency modes for each ring are shown in Figure 9. These are all p-modes.

Like the Kuzmin disk, isolated broad Gaussian rings with unsoftened gravity do not support g-modes. We have examined a sequence of Gaussian rings with  $s = 1$ , near-zero softening ( $\beta = 10^{-4}$ ), and increasing  $\lambda$ . The fundamental g-mode is well-defined for  $\lambda = 0.5$  (Figure 10), but disappears by  $\lambda = 0.59$ .

## 3.3. The Jacobs-Sellwood ring

Jacobs and Sellwood (1999) have reported two-dimensional  $N$ -body simulations of a low-mass annular disk orbiting a central mass. They were able to establish long-lived  $m = 1$  normal modes that survived with little sign of decay for over 1500 orbital periods. The surface-density distribution in the disk was

$$\Sigma_d(r) = \frac{2M_d}{\pi} [1 - 4(1 - r)^2]^{1/2}, \quad \frac{1}{2} < r < \frac{3}{2}, \quad (59)$$

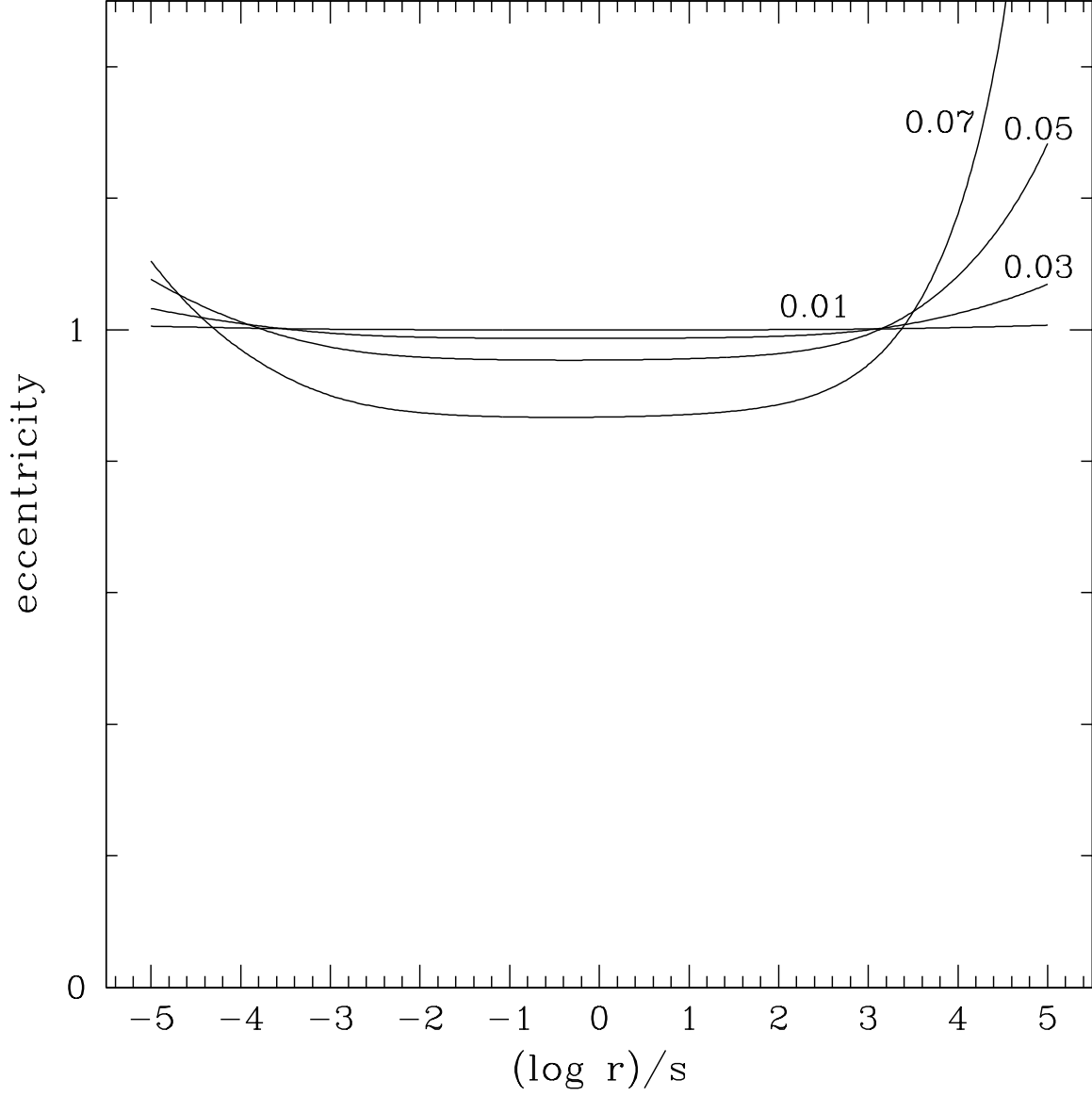


Fig. 8.— The fundamental slow modes for narrow Gaussian rings (eq. 58). The modes are normalized so that  $\int e^2(r) d\log r / \int d\log r = 1$ , and labeled by  $s$ , the dispersion in  $\log r$ . There are no slow modes for  $s > 0.07$ .

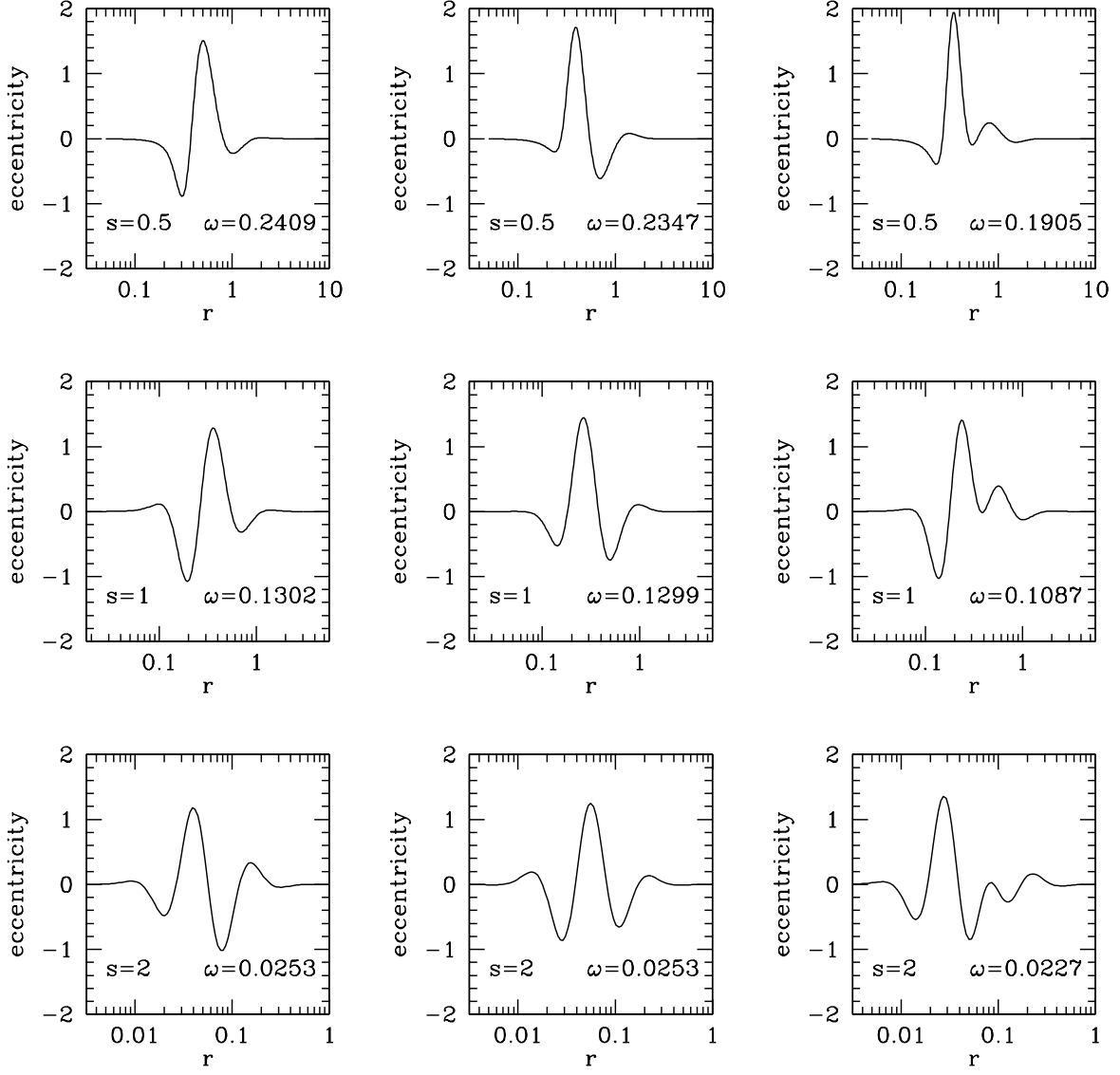


Fig. 9.— Slow p-modes in the isolated Gaussian ring (eq. 58) with softened gravity,  $\beta = 0.2$ . The panels are labeled with the width parameter  $s$  and the eigenfrequency. The scale in  $\log r$  is the same in all panels but the origin is different.



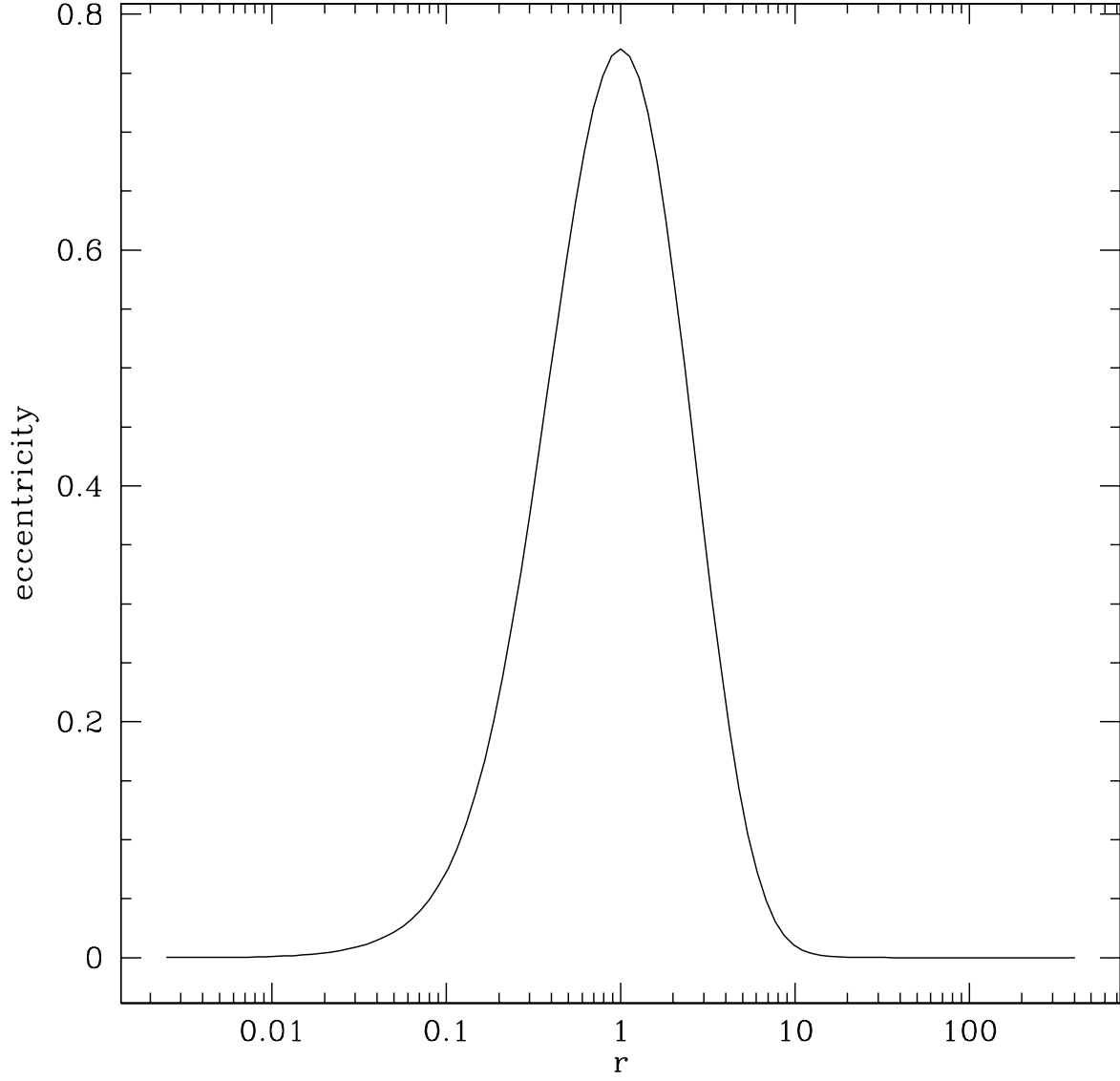


Fig. 10.— The fundamental g-mode in a Gaussian ring with width  $s = 1$  and  $\lambda = 0.5$ . Gravity is unsoftened ( $\beta = 10^{-4}$ ). The frequency of the mode is  $\omega = -0.1527$  and is proportional to the disk mass, which is here chosen to be  $M_d = 1$ .

and zero otherwise. In contrast to our other models, this disk has sharp edges at  $r_{\pm} = \frac{3}{2}, \frac{1}{2}$ , where the surface density goes to zero as  $\Sigma_d \propto |r - r_{\pm}|^{1/2}$ . To ensure that our numerical methods handle edge effects properly, we extend the ring to  $fr_+$  and  $r_-/f$ ,  $f = 1.35$ , with a very low surface-density envelope,  $\Sigma_d = 10^{-8}M_d$ .

The precession rate in the unperturbed disk (59) is shown in the left panel of Figure 11, for several values of the softening parameter  $\beta$ . The cusps at the inner and outer disk edge  $r_{\pm}$  arise because of the sharp edges.

The right panel of Figure 11 shows the frequencies of p-modes as a function of the softening parameter. The ten modes with the largest frequency are shown. The modes occur in degenerate pairs for  $\beta \ll 1$  and the degeneracy is gradually lifted as  $\beta$  increases. Each mode terminates at a maximum softening parameter, which is shown by a filled circle. For  $\beta > 0.229$  there are *no* non-singular modes.

Figure 12 shows the shape of the highest frequency (fundamental) p-mode for several values of the softening parameter. Note that for the larger softening parameters, the amplitude of the mode does not go to zero at the disk edge.

#### 4. Earlier work

Sridhar, Syer and Touma (1999) recognized the importance of slow modes in nearly Keplerian disks, and both formulated and solved numerically the linear eigenvalue problem. However, they employed the equations of Laplace-Lagrange secular perturbation theory (Murray and Dermott 1999), which is designed for planetary systems and so approximates the disk as a set of non-intersecting rings. This approach does not give the correct answers for a continuous disk, even as the number of rings becomes arbitrarily large, because it assumes that the eccentricities are small compared to the distance between rings. For example, all of the eigenfrequencies are non-negative in Laplace-Lagrange theory (Sridhar et al. 1999), whereas we have found negative eigenfrequencies in both the WKB approximation and numerical solutions.

Lee and Goodman (1999) have investigated stationary linear and nonlinear  $m = 1$  density waves in nearly Keplerian disks. They have derived the nonlinear dispersion relation in the tight-winding approximation, and found self-similar logarithmic spirals with zero frequency in the special case where the disk surface density  $\Sigma_d(r) \propto r^{-3/2}$ . In the linear limit, their self-similar spirals exhibit properties reminiscent of the results of this paper: isolated disks do not support long waves, and zero-pressure disks in an external potential only support waves if the parameter  $\lambda$  from equation (42) satisfies  $\lambda < [\Gamma(\frac{1}{4})/\Gamma(\frac{3}{4})]^4/144 = 0.53214$ , similar to our finding that there are no g-modes in the Kuzmin disk or  $s = 1$  Gaussian ring if  $\lambda \gtrsim 0.5$ –0.6.

Sridhar and Touma (1999) have examined the slow dynamics of eccentric orbits in nearly Keplerian potentials with a non-axisymmetric potential perturbation. They found two general

families of orbits, lenses and loops, and suggest that a self-consistent lopsided disk around a point mass could be assembled from aligned loop orbits. Our results extend this conclusion by showing that aligned loops generally can support self-consistent slow g-modes, but only if the precession is dominated by an external non-Keplerian potential or the disk is a narrow ring. In essence, the aligned loop orbits discussed by Sridhar and Touma work *too* well: the non-axisymmetric gravitational field that they produce is too strong for a self-consistent slow mode. The progeny of aligned loop orbits, which Sridhar and Touma (1999) call librating loop orbits, can support self-consistent p-modes in isolated disks, but large-scale p-modes require that the velocity dispersion is large.

Statler (1999) has constructed sequences of periodic orbits in the potential of a point mass plus a lopsided disk. He argues that the precession of a self-consistent lopsided disk must be prograde ( $\omega > 0$ ), and that the eccentricity  $e_K(r)$  must have a node. We find that neither of these results is generally true for g-modes: for example, the fundamental g-mode in the Kuzmin disk with  $\lambda = 0.1$  (Fig. 3) has no nodes and  $\omega < 0$ . Nevertheless, Statler’s arguments may well describe the essential dynamics of some lopsided disks.

Goldreich and Tremaine (1979) investigated slow modes in planetary rings. The thrust of their investigation was quite different, for several reasons: there was strong differential precession due to an external source (the planet’s quadrupole moment), so that uniform precession was sustained only by a strong eccentricity gradient ( $de/d\log a \gg 1$ ); the ring was very narrow ( $\Delta a/a \sim 10^{-4}$ ); the ring was sharp-edged, so that the “resonant cavity” involved reflection at the disk edges rather than at turning points in the dispersion relation; and finally, later work (Chiang and Goldreich 2000) shows that the mode properties in narrow, dense, particulate rings are strongly affected by collisions near the disk edge. In contrast, the slow modes examined here should be insensitive to the details of the disk edges since they are restricted to the interior of the disk (except for some of the modes in the strongly softened Jacobs-Sellwood ring, Figure 12).

## 5. Conclusions

Disks orbiting massive bodies support slow modes; these are linear  $m = 1$  normal modes whose eigenfrequency is proportional to the strength of collective effects in the disk, rather than to its characteristic radial or azimuthal frequencies. The most important collective effects are likely to be the self-gravity of the disk, and the velocity dispersion in collisionless disks or the pressure in fluid disks. The first two of these—and to a lesser extent the third—can be approximated by softened self-gravity (Fig. 1). Slow modes are important because these are likely to be the only large-scale or long-wavelength modes, and hence can dominate the overall appearance of the disk. Moreover, slow modes are relatively immune to damping by viscosity, Landau damping, collisions, or other dissipative mechanisms.

Slow modes in which the disk self-gravity is the dominant collective effect are described by

the same equations used in the classic Laplace-Lagrange secular perturbation theory for planetary systems, except that (i) the number of planets  $N$  goes to infinity and the mass per planet  $m \propto N^{-1}$ ; (ii) the Laplace-Lagrange equations are valid in the limit where the planets’ radial excursions are much less than their radial separation, whereas in continuous disks the radial separation of the mass elements is smaller than the radial excursions. The simplest way to modify Laplace-Lagrange theory to account for this difference is to soften gravity.

We have derived the eigenvalue equation (42) that describes slow modes in a nearly Keplerian disk with softened gravity. We have solved this equation numerically to investigate the properties of modes in the Kuzmin disk (eq. 4), the Gaussian ring (eq. 58), the Jacobs-Sellwood ring (eq. 59), and a variety of other disks not reported here. Many of our results can be interpreted in the framework of the WKB approximation (§1.3). Our conclusions can be summarized as follows:

1. All slow modes have real frequency, and thus are stable.
2. There are two main types of discrete slow mode: (i) g-modes involve long leading and long trailing waves. Their properties are insensitive to the softening parameter  $\beta$  once it is sufficiently small. In general these are retrograde (eigenfrequency  $\omega < 0$ ). The fundamental g-mode has zero nodes, the lowest eigenfrequency, and a scale comparable to the disk radius. (ii) The properties of p-modes depend on the softening parameter; in particular their characteristic wavenumber is  $k \sim \pm\beta/r$ . In the WKB approximation that is valid for  $\beta \ll 1$ , p-modes come in degenerate pairs, one composed of short and long trailing waves and the other of short and long leading waves. In general p-modes are prograde ( $\omega > 0$ ), and the fundamental p-mode has the largest  $\omega$ .
3. Narrow rings have a trivial slow g-mode,  $e_K(r) = \text{constant}$ . We have examined a wide variety of broad rings and disks, but have found none that support g-modes when they are isolated. In the presence of an external non-Keplerian potential that supplies a fraction  $1 - \lambda$  of the total precession, a variety of disks appear to support g-modes if and only if  $\lambda \lesssim 0.5\text{--}0.6$ .
4. The p-modes are modulated at the characteristic spatial frequency  $k_0 = \beta/r$ . Thus long-wavelength p-modes occur only in disks with substantial softening (cf. Figures 6, 9, and 12).
5. In general disks support a finite number of discrete normal modes and a continuum of singular modes. In some cases, such as the Jacobs-Sellwood ring with  $\beta > 0.229$ , there are no discrete normal modes.

Of course, these models have many shortcomings: they are linearized; they use softened gravity as a crude proxy for velocity dispersion or pressure; and the softening law (eq. 50) was chosen for mathematical convenience and does not correspond to a simple interparticle force law. The models also do not address the important questions of how rapidly slow modes damp (although the N-body

simulations of Jacobs and Sellwood 1999 suggest they can be very long-lived), or how large the disk-mass ratio  $M_d/M$  can be in disks that support discrete slow modes. To decide these issues there is no substitute for careful  $N$ -body simulations; however, our results provide a guide for interpreting these simulations. This paper also does not address the question of how slow modes are excited and whether long-lived slow modes actually play a significant role in the structure and evolution of a variety of astrophysical disks.

I thank Kathryn Johnston for a number of stimulating early discussions of this problem, and Jerry Sellwood and Alar Toomre for thoughtful comments. This research was motivated and guided by the simulations of eccentric disks carried out by Vince Jacobs and Jerry Sellwood, and I thank them for sharing their results freely. This work was supported in part by NSF grant AST-9900316 and NASA Grant NAG5-7310.

## REFERENCES

- Binney, J., and Tremaine, S. 1987, *Galactic Dynamics*, Princeton: Princeton University Press
- Chiang, E. I., and Goldreich, P. 2000, *ApJ*, 540, 1084
- Courant, R., and Hilbert, D. 1953, *Methods of Mathematical Physics*, Vol. I, New York: Interscience
- Erickson, S. A. 1974, Ph.D. thesis, Massachusetts Institute of Technology
- Goldreich, P., and Tremaine, S. 1979, *AJ*, 84, 1638
- Jacobs, V., and Sellwood, J. A. 1999, in *Galaxy Dynamics*, eds. D. Merritt, J. A. Sellwood, and M. Valluri, San Francisco: Astronomical Society of the Pacific, 39
- Kalnajs A. J. 1965, Ph.D. thesis, Harvard University
- Lee, E., and Goodman, J. 1999, *MNRAS*, 308, 984
- Lin, C. C., and Shu, F. S. 1966, *Proc. Nat. Acad. Sci.*, 55, 229
- Miller, R. H. 1971, *Ap&SS*, 14, 73
- Murray, C. D., and Dermott, S. F. 1999, *Solar System Dynamics*, Cambridge: Cambridge University Press
- Press, W. H., Teukolsky, S. A., Vetterling, W. T., and Flannery, B. P. 1992, *Numerical Recipes*, 2nd ed., Cambridge: Cambridge University Press
- Safronov, V. S. 1960, *Ann. d’Ap.*, 23, 979
- Shu, F. H., Tremaine, S., Adams, F. C., and Ruden, S. P. 1990, *ApJ*, 358, 495

- Sridhar, S., and Touma, J. 1999, MNRAS, 303, 483
- Sridhar, S., Syer, D., and Touma, J. 1999, in *Astrophysical Discs*, eds. J. A. Sellwood and J. Goodman, San Francisco: Astronomical Society of the Pacific, 307
- Statler, T. S. 1999, ApJ, 524, L87
- Toomre, A. 1964, ApJ, 139, 1217
- Toomre, A. 1969, ApJ, 158, 899
- Toomre, A. 1977, ARA&A, 15, 437

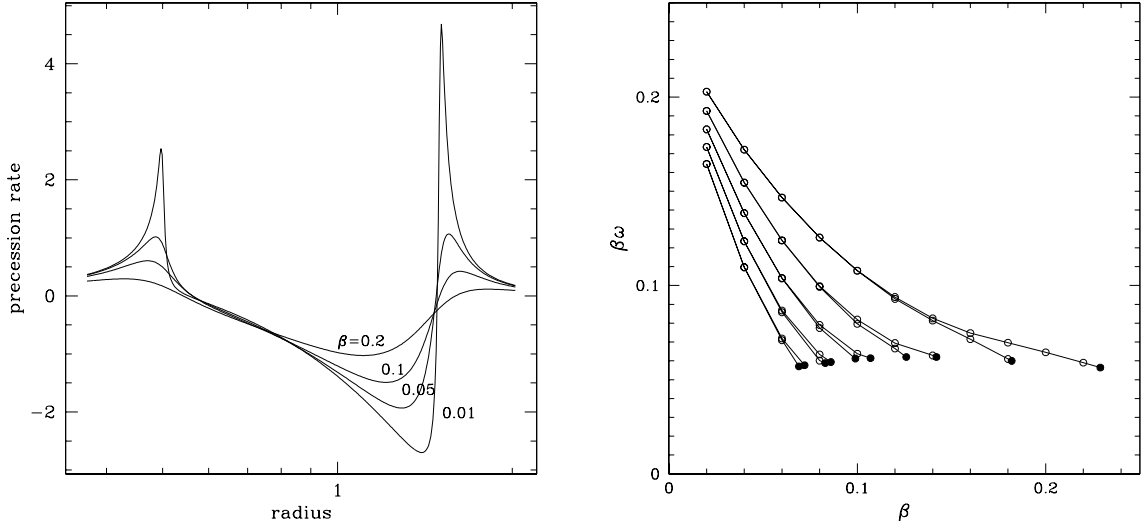


Fig. 11.— (Left) The apsidal precession rate for the Jacobs-Sellwood ring (eq. 59) for softening parameter  $\beta = 0.01, 0.05, 0.1, 0.2$ . (Right) Slow p-modes in the isolated Jacobs-Sellwood ring with softened gravity. We show the ten modes with the highest frequency. The modes occur in degenerate pairs when  $\beta \ll 1$ . Each mode terminates at a maximum softening parameter, shown by a filled circle. The units are chosen so that  $G = M = M_d = 1$ , and  $\omega \propto M_d$ .

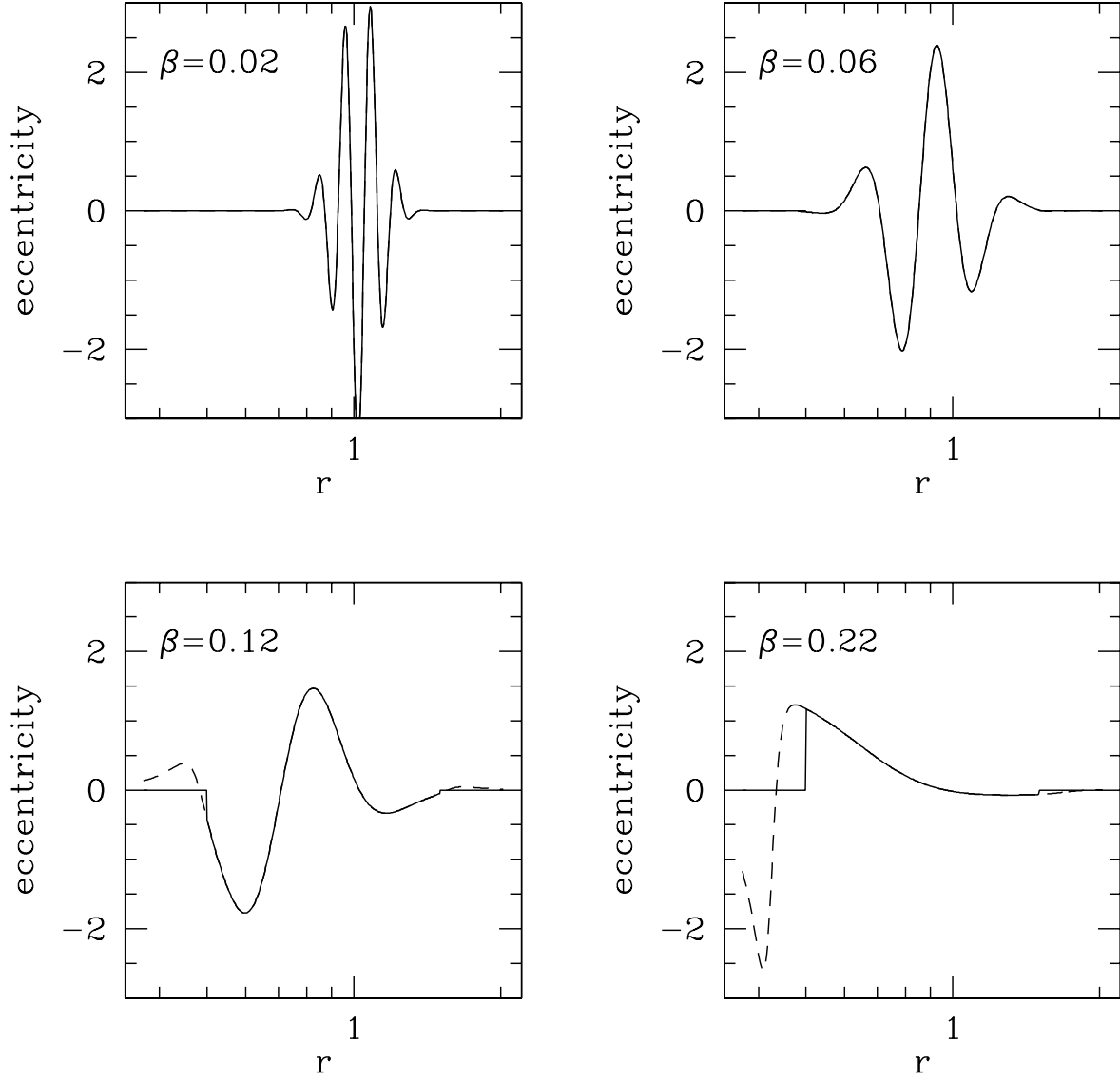


Fig. 12.— The p-mode in the Jacobs-Sellwood ring with the highest frequency, for  $\beta = 0.02, 0.06, 0.12, 0.22$ . The dashed lines show the amplitude of the mode in the a low surface-density envelope ( $\Sigma_d = 10^{-8} M_d$ ) that surrounds the ring in our numerical model.